Stability of $Cu_2ZnSnSe_4$/CdS heterojunction based solar cells under soft post-deposition thermal treatments

Fabien Atlan[1], Ignacio Becerril-Romero[1], Sergio Giraldo[2], Victoria Rotaru[2,4], Yudania Sánchez[1], Galina Gurieva[3], Susan Schorr[3,5], Ernest Arushanov[4], Alejandro Pérez-Rodríguez[1,6], Victor Izquierdo-Roca[1,*] and Maxim Guc[1,*]

[1]*Catalonia Institute for Energy Research (IREC), Jardins de les Dones de Negre 1, 2ª pl., 08930 Sant Adrià del Besòs Barcelona, Spain*

[2]*Photovoltaic Group, Departament d'Enginyeria Electrònica, Universitat Politècnica de Catalunya (UPC), Barcelona, 08930, Spain.*

[3]*Department Structure and Dynamics of Energy Materials, Helmholtz-Zentrum Berlin fur Materialien und Energie, Helmholtz-Zentrum Berlin für Materialien und Energie Hahn-Meitner-Platz 1, 14109 Berlin, Germany*

[4]*Institute of Applied Physics, Academiei Str. 5, MD-2028 Chisinau, Republic of Moldova*

[5]*Institute of Geological Sciences, Freie Universitat Berlin, Malteserstraße 74-100, 12249 Berlin, Germany*

[6]*Departament d'Enginyeria Electrònica i Biomèdica, Universitat de Barcelona, Martí i Franquès 1, 08028 Barcelona, Spain*

**Corresponding authors: V.I.-R. <vizquierdo@irec.cat>; M.G. <mguc@irec.cat>*

Abstract

The thermal stability of the $Cu_2ZnSnSe_4$ (CZTSe) absorber and CdS buffer layers in SLG/Mo/CZTSe/CdS/i-ZnO/ITO devices is explored by performing a series of soft (~200 °C) post deposition treatments (PDTs). A comprehensive analysis of a sample comprised by 56 individual devices by means of Raman and photoluminescence spectroscopies coupled with optoelectronic characterization is performed at different PDT steps. This allows isolating the effects of the PDT on the CZTSe absorber and CdS buffer layer separately and reveals clear evidences of: i) a degradation of the absorber due to Cu/Zn disorder that hinders device performance, and ii) an improvement of the buffer layer by the recrystallization of the CdS nanolayer that is the main responsible for the PDT-induced efficiency improvement. As such, it is concluded that CZTSe/CdS based PV devices present a low thermal stability under relatively low temperatures (in the 100 – 200 °C range), comparable to the temperatures employed at the final production stages of thin film PV devices or even during device operation, that leads to significant changes in solar cell performance and needs to be taken into consideration for the further development of the kesterite PV technology. These results are

supported by a novel methodology for easily discerning between changes in Cu/Zn disorder and in point defects concentration in kesterites based on solely on Raman spectroscopy that is proposed in this work and developed through the analysis of a set of CZTSe powder samples with strong variation of the order parameter Q.

Keywords: kesterite, solar cell, thermal stability, Cu/Zn disorder, CdS recrystallization

1. Introduction

The most successful inorganic thin film photovoltaic (PV) technologies, $Cu(In_{1-x}Ga_x)Se_2$ (CIGS) and CdTe, with record efficiencies beyond 20 %, rely on scarce and toxic elements [1,2]. This will inevitably limit their future production throughput [3-5] and decrease their energy return on investment (EROI) preventing them to be a feasible alternative to fossil fuels to power society [6]. In this regard, $Cu_2ZnSn(S_xSe_{1-x})_4$ (CZTSSe or kesterite) compounds represent a promising Earth-abundant and low toxicity alternative for thin film PV with higher potential for long-term mass production. However, the record efficiency of this technology at laboratory scale has been stagnated at 12.6 % since 2014 [7], with insignificant improvements of the certified efficiency in the last years [8]. In the quest towards efficiency improvement in kesterite solar cells and inspired by the positive results obtained for CIGS [9-14], it has been found that post-deposition treatments (PDTs) at low temperatures (usually <300 ºC) may boost the performance of CZTSSe-based devices. In this regard, there are two main experimental approaches: i) to perform the PDT on the bare kesterite absorber, and ii) to perform the PDT on the kesterite/CdS heterojunction or on complete devices including also the front contact layers.

In the case of the PDTs on the bare kesterite absorber, these are mostly performed in air and combined with chemical etchings (to remove the resulting secondary phases from the absorber surface), and have been proven to be an effective approach for improving the optoelectronic quality of kesterite absorbers [15-26]. The beneficial effects on device performance of this type of PDT are usually claimed to arise from changes in the ordering degree (especially, Cu/Zn disorder) of the absorber [20-22] or to other effects such as Na diffusion, surface composition modification or grain boundary passivation [15,16,18,23].

As for the PDT applied to the heterojunction or complete devices, which is the main scope of the present work, beneficial effects have been reported for pure Se (CZTSe) (e.g. Refs. [18] and [27-29]), pure S (CZTS) (e.g. Refs. [30-33]) and CZTSSe solid solution (e.g. Refs. [34-36]) based kesterite devices, with the best results obtained when the devices are annealed in air. In this case, besides affecting the kesterite absorber in comparable ways to when performed on the

bare absorber (such as improved Cu/Zn order-disorder), the PDT of the heterojunction and full devices also induces: i) element interdiffusion at the interfaces (mainly at the kesterite/CdS interface) that may modify composition and/or band alignment, and ii) intrinsic modifications in the CdS and front contact layers. For CZTS, many of the benefits of the PDT are commonly ascribed to the achievement of a more favorable band alignment with the CdS (from cliff- to spike-like) at the interface as a result of element interdiffusion and the formation of intermediate interface layers (e.g. $Zn_{1-x}Cd_xS$ or $Cu_2(Zn,Cd)SnS_4$) which usually requires high PDT temperatures (>300 ºC) [31,37]. As for CZTSe, our previous investigation of soft thermal treatments of CZTSe-based solar cells suggested that the changes induced by the PDT are mainly related to variations in defect concentration at the absorber surface and sub-surface regions [18,29]. Finally, for CZTSSe-based devices, a combination of both effects (improved alignment and changes in defect concentration) has been reported [34]. Nevertheless, with such a complex stack of thin film layers, the effect of soft PDTs on the individual layers of a CZTSSe-based thin film full solar cell, and especially on their thermal stability, is still under discussion and requires further detailed analyses.

In this context, the present work provides a thorough analysis of soft (~200 ºC) PDTs on a CZTSe/CdS sample comprised by 56 individual devices in which the effects of the PDT on the CZTSe absorber and CdS buffer layer are isolated from each other. Through the combination of J-V, Raman and photoluminescence analyses, the thermal stability of each layer is studied in detail revealing that the main device performance benefits provided by the PDT arise exclusively from the improvement of the CdS crystallinity while significant Cu/Zn disorder and a slight increase in defect concentration are induced throughout the whole CZTSe absorber layer resulting in a slightly negative effect on device efficiency. These conclusions are based on a new Raman-based methodology that is also proposed in this work and that enables to distinguish between changes in defect concentration and in Cu/Zn disorder in CZTSe absorber based solely on spectroscopic data.

2. Experimental details

2.1 Sample preparation

In order to provide a deep understanding of the effect of soft PDTs on the CZTSe absorber and on the CdS buffer layers, two different sets of samples were employed in this study. The first one consisted in full CZTSe devices fabricated on soda-lime glass (SLG) that were analyzed before and after being submitted to PDT processes. The second one consisted in a set of high

quality CZTSe powder with different PDT conditions yielding different Cu/Zn disorder states. These are described in detail below.

2.1.1 PDT of CZTSe devices. A SLG/Mo/CZTSe sample (5×5 cm^2) was synthesized following a sequential process based on the sputtering of Mo/Cu/Sn/Cu/Zn metallic precursor stacks and their subsequent selenization in a tubular furnace through a reactive annealing in [Se]+[Sn] atmosphere (the full details of the process are described in Ref. [38]). The composition of the different layers was measured by X-ray fluorescence (Fischerscope XDV) and chosen to be Cu-poor and Zn-rich ([Cu]/([Zn]+[Sn]) = 0.72 and [Zn]/[Sn] = 1.08) since this has been proven to be a requirement for high efficiency kesterite devices [39].

The sample was finalized through the deposition of the top layers:

- CdS deposition: CdS buffer layer deposited by chemical bath deposition (CBD) with a slow growth rate (~1 nm/min in average) which ensures a homogeneous and compact coverage of the absorber layer and a high reproducibility (full details of the process can be found in Ref. [40]).
- Front contact deposition: i-ZnO (50 nm)/ITO (200 nm) front contact deposited by pulsed DC-magnetron sputtering (Alliance Concept CT100) with no intentional substrate heating. Since the present study focuses on the influence of soft PDTs on the CZTSe and CdS layers, especial care was put into ensuring that the temperature of the sample during this process did not exceed 50 °C.

Once finished, the sample was mechanically scribed into 3×3 mm^2 individual solar cells and cut into two pieces: i) a main sample containing 56 devices, and ii) a control sample containing 16 devices. The relatively high number of devices in the samples allows extracting statistically reliable conclusions in the analyses performed throughout the work.

In order to study the effect of soft PDTs on the CZTSe devices and discern between the absorber- and CdS-related effects, the following experimental procedure was followed (see the schematic representation in Figure 1):

1. The "*As-deposited*" main sample was submitted to a first PDT (*PDT-1*) performed in a hot plate in air at ~200 °C during 25 min ➔ By analyzing the devices before and after the PDT, the combined effects of the PDT on the absorber and CdS layers were studied.
2. The CdS and front contact layers were removed through an HCl (~15% (w/w)) etching and new "fresh" layers were deposited in identical conditions to the original ones in both the main and control samples (*New top*) ➔ This allowed to: i) study the effect of the PDT

only on the annealed absorber (main sample) and, ii) study the possible additional effects of the HCl etching on the absorber and on the properties of the new CdS layer (control sample).

3. The main sample was submitted to a second PDT (*PDT-2*) identical to that performed in step 1 ➔ This allowed to isolate the effect of the PDT on the CdS.

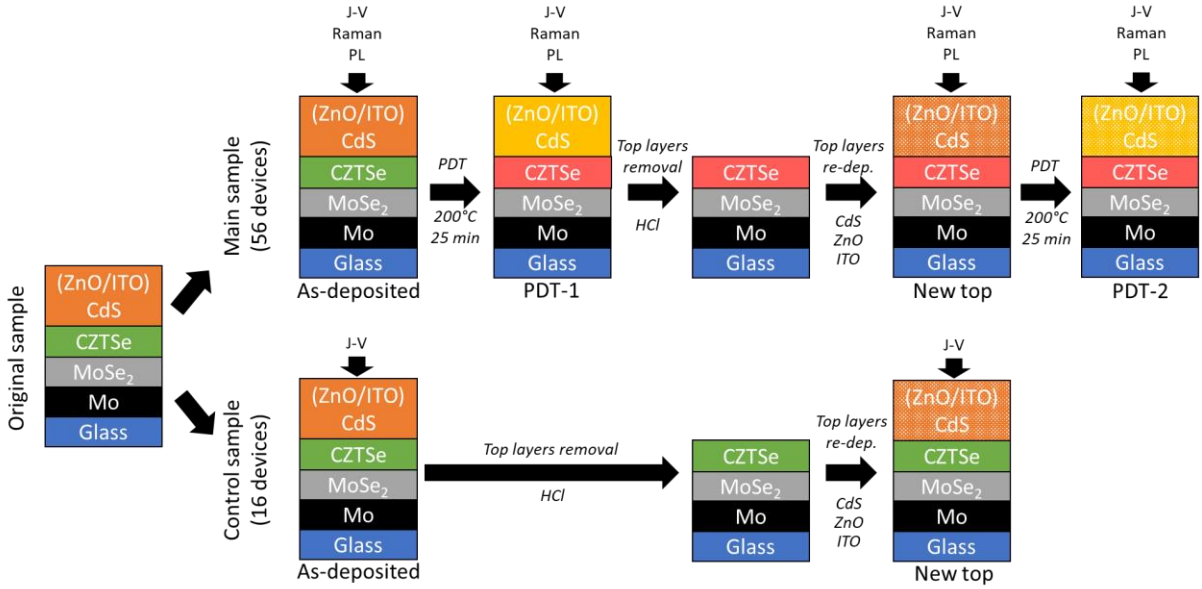

Figure 1. *Scheme of the different post deposition treatment steps performed in the present study. See the text for the details of each step.*

In this way, the procedure carried out allowed clearly separating the effect of soft thermal treatment on the absorber and buffer layers, and to define strictly the thermal stability limitations for each of them.

2.1.2 High quality CZTSe powder with different PDT. In order to provide a deeper insight into the origin of the effects of the PDT on the CZTSe absorbers and their possible relation with Cu/Zn disorder, a separate set of high quality CZTSe powder samples was used. The samples of this set were exposed to different annealing temperatures with an immediate quenching, which resulted in a strong variation of the order parameter Q, which was defined by anomalous X-ray powder diffraction (see Ref. [41] for information about the synthesis of the samples and additional analysis).

2.2 Characterization

The effect of the PDT on the J–V characteristics of the CZTSe devices at the different steps described in the previous sub-section was studied under simulated AM1.5 illumination (1000 W/m^2 intensity at room temperature) using a pre-calibrated Sun 3000 Class AAA solar simulator (Abet Technologies).

On the other hand, the main technique employed for the detection of the changes related to the soft thermal treatment in different layers of the solar cells was Raman scattering spectroscopy. This technique already showed an impressive potential to detect different structural, compositional and defect related variations in multinary compounds in general [42-45] and in kesterite type compounds in particular [25,46-48]. Moreover, Raman spectroscopy is a fast and non-destructive technique, and by varying the excitation wavelength allows to analyze different layers in already completed devices [42,46]. In this way, Raman spectroscopy was employed to analyze the presence of secondary phases and point defects in the macro scale at the front and back (after detaching the absorber from the substrate through a mechanical lift-off process) sides of the sample. An FHR640 Horiba Jobin Yvon spectrometer coupled to a Raman probe developed at IREC and a CCD camera was used. Laser excitation wavelengths of 442 nm (for CdS analysis) and 532 nm (mainly for CZTSe analysis) were employed in backscattering configuration. A laser power density of about 150 W cm^{-2} was used to prevent thermal effects on the samples and the diameter of the laser macro-spot was around 70 μm. The Raman shift was calibrated using a monocrystalline Si reference by imposing the position of its main peak to be at 520 cm^{-1}. An unpolarized laser beam was used to minimize the impact of the crystalline orientation in the Raman spectra.

Photoluminescence (PL) was also performed on the samples with laser excitation of 785 nm and an *i*HR320 Horiba Jobin Yvon spectrometer with a probe designed in IREC and an InGaAs camera. The laser power density and spot size were similar to those employed for Raman spectroscopy with the 442 and 532 nm excitations as described above.

Finally, anomalous X-ray powder diffraction was employed to determine the Q order parameter in the high quality CZTSe powder samples. Details about the measurement conditions and data analysis can be found in Ref. [41].

3. Results and discussions

3.1 Evaluation of the optoelectronic properties under soft PDTs

The impact of each soft PDT treatment step was first defined by analyzing the optoelectronic properties of the solar cells. For this, the J-V curves of the 56 solar cells of the main CZTSe sample (see PDT of CZTSe devices) were analyzed at the main steps of the PDT experimental procedure (see Figure 1). The evolution of the optoelectronic parameters is presented in Figure 2. The first observation that can be made from the results is that there is a clear increase in device performance (~20 % relative in average efficiency) with the first soft PDT (i.e. *As-*

Deposited vs *PDT-1*). However, after the re-deposition of the CdS and front contact layers (*New top*) the performance of the devices drops by almost 50 % presenting efficiencies significantly lower than even the original *As-Deposited* sample. Finally, the realization of a second PDT (*PDT-2*) allows recovering similar efficiency values as those obtained after the first PDT. In order to verify the possible influence on device performance of the HCl etching process employed for the removal of the CdS and front contact layers, the J-V characteristics of the control sample in "As-deposited" conditions and after the re-deposition of the top layers were studied and the results are displayed in Figure S1. In this case, no significant difference was found in the average values of the different optoelectronic parameters, with only an increase of the dispersion of V_{oc} and FF after the top layers re-deposition. This allows to infer that the decrease of the optoelectronic parameters from the *As-Deposited* to the *New top* steps of the experimental procedure are directly related to the PDT-treatment of the CZTSe absorber with a negligible influence of the HCl etching process or the new CdS and front contact layers.

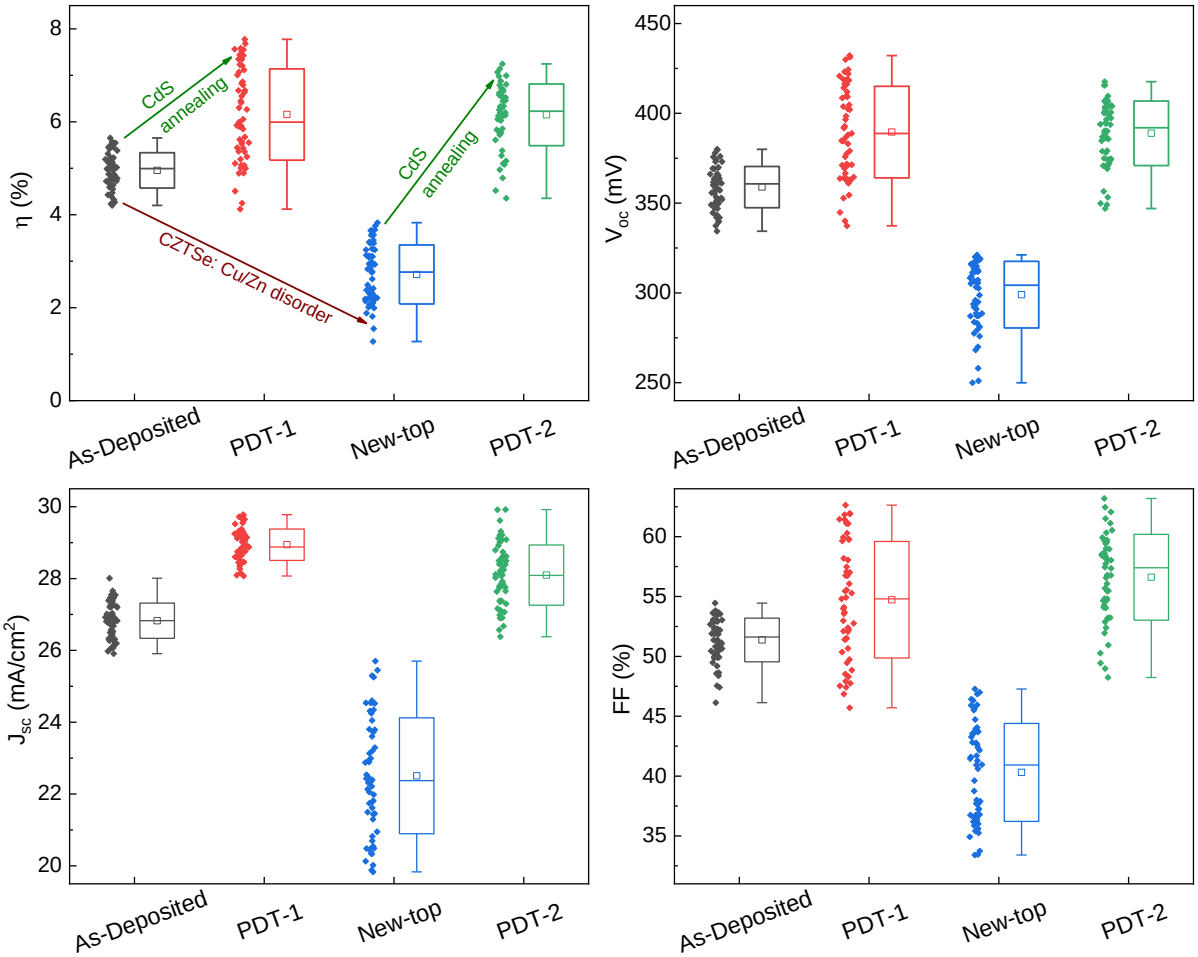

Figure 2. *Evolution of the optoelectronic parameters of the SLG/Mo/CZTSe/CdS/i-ZnO/ITO solar cells before and after the soft thermal treatments.*

Furthermore, as follows from Figure 2, in all the cases, the efficiency variations observed arise from a similar variation of all the optoelectronic parameters (V_{oc}, J_{sc} and FF) of the devices

denoting significant changes both in bulk and at the interfaces of different layers as a consequence of the soft PDT. However, the fact that the PDT-treated absorber with untreated CdS (i.e. *New top*) presents the worst performance implies that the PDT-induced modifications of the CdS and/or the absorber/buffer interface are the main responsible for the device efficiency improvement. Taking into account that the front contact layers (i-ZnO/ITO) were deposited with insignificant heating of the substrate (see PDT of CZTSe devices), it is worth noticing that the standard deposition conditions used by different groups for the deposition of these layers may hinder the effect of soft PDTs [49-54]. Nevertheless, as pointed out in the Introduction, the effect of such a PDT on the different layers of CZTSe solar cells and, especially, on their thermal stability, is still under discussion and requires a more detailed analysis beyond the J-V characteristics. This is the main objective of the following sections of the present study.

3.2 Thermal stability of the CZTSe absorber layer

In order to deepen into the effects of the PDT in the CZTSe absorber layer, the 56 devices of the main sample were analyzed by Raman spectroscopy under green excitation wavelength (532 nm) at the main steps of the PDT experimental procedure (see Figure 1). The resulting Raman spectra are displayed in Figure 3 (the 56 spectra are displayed as a pale diffuse spectral cloud curve and the average spectrum is shown as a legible solid line). The Raman scattering spectra of the *As-Deposited* solar cells (black curve in Figure 3a) show the typical shape for a CZTSe compound with good crystalline quality [46]. The main LO peak of the CdS can also be seen in the spectra at ~300 cm^{-1}, but its intensity is significantly lower than that of the kesterite peaks. After applying the first PDT (red curve in Figure 3a), a significant change of the relative intensity of the CdS peak can be seen which can be attributable to an improved crystallinity as will be discussed later on. The variations in the spectrum of the CZTSe layer after the PDT are less pronounced. However, the relatively high amount of solar cells analyzed in this work enables to detect clear differences in the average spectra before and after the PDT. These are characterized by the decreased relative intensity of the peaks close to 170 cm^{-1} (here the band is comprised by two A symmetry peaks and of a B symmetry peak), by the increased relative intensity of the peaks at high wavenumber (210 – 260 cm^{-1}, comprised by several E and B symmetry peaks), and by the increased asymmetry of the main A_1 symmetry peak of CZTSe [55]. After the etching and re-deposition of the buffer and window layers (*New top*) the relative intensity of the CdS peak becomes similar to that of the *As-Deposited* step, while the shape of the CZTSe Raman spectra do not show detectable changes compared to the *PDT-1* step. The latter is in line with the absence of any effect of the HCl etching on the absorber observed also

in the Evaluation of the optoelectronic properties under the soft thermal treatment. After the second PDT is performed on the devices with the re-deposited CdS and front contact, the changes in the Raman peaks related to CZTSe are similar to those observed in *PDT-1* but with a less pronounced effect, denoting a possible saturation.

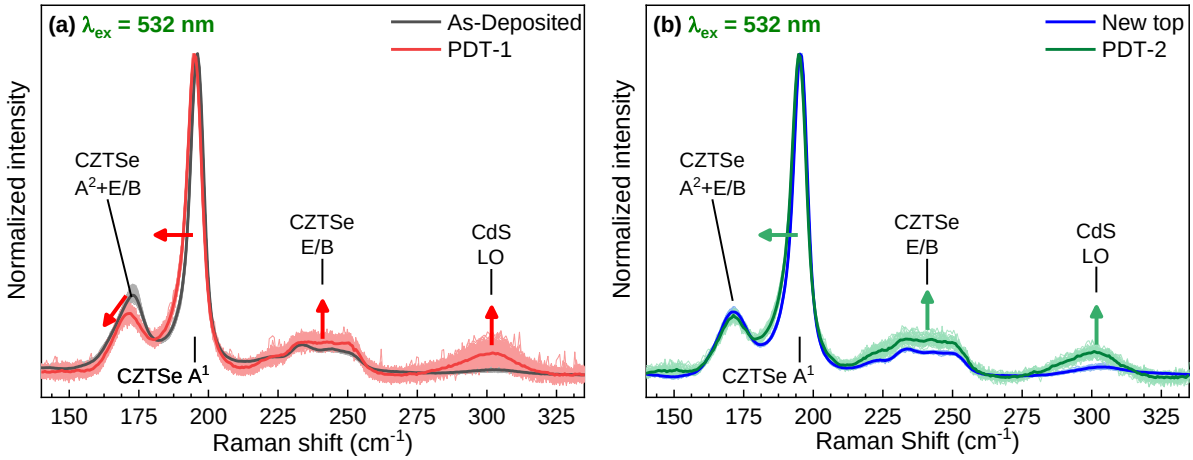

Figure 3. *Raman scattering spectra of SLG/Mo/CZTSe/CdS/i-ZnO/ITO solar cells measured under green excitation wavelength at steps (a) As-deposited and PDT-1 and (b) New top and PDT-2. Here the pale lines (resulting in a pale diffused spectral cloud) represent the individual spectra of the 56 analyzed cells and legible solid lines are the average of all spectra.*

Previously, similar variations of the Raman spectra of CZTSe compounds were observed when the chemical composition of the thin films varied and were shown to be directly related to changes in the amount of different point defects or defect clusters in the kesterite type structure [47,56]. Moreover, our previous investigation on soft PDTs in CZTSe-based solar cells assumed that these effects in the Raman spectra were mainly caused by changes of the defects at the absorber surface and sub-surface regions [57]. However, in the present study, the Raman spectra of CZTSe-based solar cells before and after the PDT were also measured at the back interface of the absorber layer after its mechanical lift-off showing similar spectral variations (see Figure S2). As such, it is likely that similar variations in defect concentration occur throughout the whole bulk of the absorber taking into account the micrometric thickness of the layer. Moreover, a close look at the various changes that appear in the spectra of the CZTSe-based devices, both in the present study and in Ref. [57], does not allow to directly assign them only to variations in defect concentration. In this respect, Ref. [56] shows an exhaustive Raman analysis of a compositionally-graded CZTSe sample, where the same thermal treatment was applied to the whole sample and, thus, the expected variations in the Raman spectra were related only to changes in defects. This work allowed defining a model of the specific features of the Raman spectra that change with the increasing defect concentration. Two main effects relevant for the present work were observed: i) changes along the A-type off-stoichiometric line (see

Ref. [46] for details about off-stoichiometric types of kesterite compounds) which correspond to changes of the [Zn_{Cu}+V_{Cu}] cluster defects and that only influence the peaks close to 170 cm^{-1} decreasing their intensity with the increasing defect concentration; and ii) spectral changes with the varying [$2Zn_{Cu}$+Zn_{Sn}] defect cluster along the B-type off-stoichiometric line which present a more complex behavior but mainly influence the peaks close to 170 cm^{-1} (relative intensity decreases with the increasing defect concentration), the peaks in the 210 – 250 cm^{-1} range (relative intensity increases with the increasing defect concentration) and the main peak at 195 cm^{-1} (small increase of the full width at the half maximum (FWHM) with the increasing defect concentration) [56]. Even the combination of these two contributions does not account for the changes observed in the absorber layer subjected to the soft PDT in the present study and in the Ref. [29]. Taking into account that the Raman spectra exhibit similar variations both at the front and back interfaces and that these do not directly correspond to off-stoichiometry changes in the kesterite absorber, it can be safely assumed that Cu/Zn disorder is the main responsible for the observed variations. Detailed discussions on how to differentiate the two effects (point/cluster defect and Cu/Zn disorder influence) using Raman spectra are presented in the following sub-section.

To complete the study about the thermal stability of the CZTSe-based solar cells, the PL spectra of the devices were analyzed at the main steps of the PDT experimental procedure (see Figure 1). The results are displayed in Figure 4 (as in the case of the Raman spectroscopy analysis, the spectra of the 56 devices appear as a pale diffuse spectral cloud curve and the average spectrum is shown as a legible solid line). After the *PDT-1*, the spectra shift to lower energies comparing to the *As-Deposited* devices (Figure 4a). This is in agreement with previously published results where the PL spectra of ordered and disordered kesterite type compounds were analyzed [26,41,57,58] and supports the assumption of the soft PDT increasing Cu/Zn disorder in the CZTSe absorber. The observed redshift of the PL maximum is explained by the shrinkage of the band gap, usually observed in disordered kesterite compounds [26,57-59].

After the etching and re-reposition of the CdS and front contact layers (*New top*), the PL spectra do not exhibit significant changes (blue line in Figure 4b). Finally, the *PDT-2* resulted in a further redshift of the PL band maximum. However, the shift is smaller than after the first PDT, which is in agreement with the smaller changes in the Raman spectra and the possible saturation of the order-disorder transition mentioned above. The same red shift tendency can also be clearly observed in Figure 4c that displays the changes in the PL band maximum. As mentioned before, the red shift of the PL band maximum after the PDTs is ascribed to the shrinkage of the band gap due to the increased Cu/Zn disorder. The redshift of the PL band maximum after the

first PDT (*PDT-1*) (~60 meV average) is lower than the total expected shift found for a complete order/disorder transition (~110-130 meV) [26,41]. This indicates that CZTSe absorber is probably transitioning from a partially ordered (before PDT) to a more disordered (after PDT) state without reaching the order-disorder limits, which is in agreement with the Raman scattering analysis as will be discussed below. After the second soft annealing step (*PDT-2*), the further redshift of the PL band maximum saturates into a total shift of ~100 meV, slightly lower than the expected shift to a complete order/disorder transition. However, the original slightly disordered state of the absorber may account for this 10 – 20 meV difference implying that the system saturates into a fully disordered state after the second PDT.

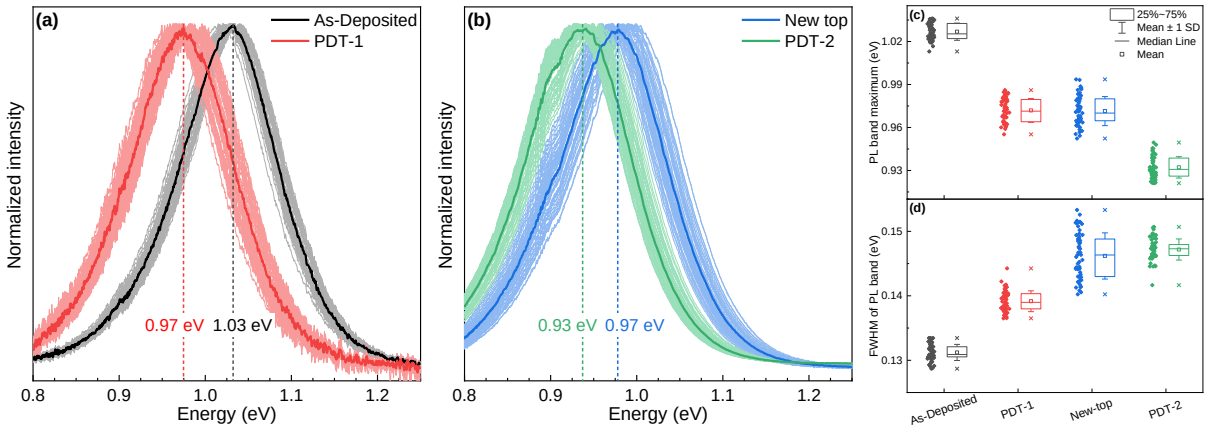

Figure 4. *PL spectra of SLG/Mo/CZTSe/CdS/i-ZnO/ITO solar cells measured under green excitation wavelength at steps (a) As-deposited and PDT-1 and (b) New top and PDT-2. Evolution of the (c) PL band maximum and of the (d) FWHM of the PL band.*

On the other hand, the change of the FWHM of the PL band at different steps is presented in Figure 4d. A continuous increase of the FWHM that saturates at the last step can be observed. This slight increase FWHM of the PL band in kesterite type compounds was ascribed to the increase of the width of the defect level involved in radiative recombination [60]. Furthermore, the influence of the thermal treatments to the width of this defect level (or even defect band) was previously observed in Cu_2ZnSnS_4 thin films [61], and is in agreement with the results of the present study. While this effect may be clear for the PDT process, the increase of the FWHM of the PL band after the etching and re-deposition of the buffer and front contact layers is not so obvious and may be related to other effects that can be a subject of further investigations.

3.3 Methodology for the evaluation of Cu/Zn disorder and defect evolution in CZTSe

As mentioned in the previous sub-section, it is key for the analysis of the thermal stability of CZTSe absorber layer under soft PDT to be able to separate the effects on the density of point/cluster defects from those arising from the Cu/Zn order-disorder transition. First of all, it has to be specified that separating these two parameters and their influence on the

physicochemical properties of kesterite absorbers is not a trivial problem, especially in case of thin film samples. However, from the point of view of Raman spectroscopy, these two effects can have slightly different effects on the obtained spectra:

- Density of point/cluster defects ➔ In case of kesterite type compounds, this is mainly related to vacancies and substitutions [62,63] and will have a direct influence on the amount of specific bonds that originate specific Raman peaks. Thus, a change in the density of defects is expected to produce mainly changes in the intensity of the Raman peaks. This type of changes have already been observed in Refs. [47,48] and [56], where the changes in defect concentration arose from variations in the deposition conditions.
- Cu/Zn order-disorder ➔ The order-disorder transition implies that the amount of involved Cu-Se and Zn-Se bonds remains similar, but length of these bonds might be slightly changed due to different surrounding atoms for the 2*c* and 2*d* Wyckoff positions (the two positions which participate in the disorder process) [41]. This type of changes result in a shift of the Raman peaks. This effect has been well described for the Cu_2ZnSnS_4 kesterite type compound [64,65].

It is worth noticing that in the case of point/cluster defects formation a shift of the Raman peaks or even significant changes in the Raman spectra cannot be excluded for a significantly large amount of defects (e.g. similar to the ordered defect compound formed in highly defective CIGS [66]), although this has not been yet reported in the literature.

In order to perform a stricter study of the effect of Cu/Zn disorder on the Raman spectra of the CZTSe kesterite type compound, a separate set of powder samples submitted to different PDT conditions resulting in strong variations of the order parameter Q (see *Experimental details*) was analyzed by Raman spectroscopy. The resulting Raman spectra are presented in Figure 5. From the figure, variations in mainly three features can be observed with the increasing PDT temperature (i.e. increasing disorder or decreasing Q parameter): i) decrease of the relative intensity of the peaks close to 170 cm^{-1}; ii) increase of the intensity of the peaks in the 210 – 260 cm^{-1} range; iii) increase of the asymmetry of the main A_1 peak together with a slight redshift. The changes in all of these features become clear at annealing temperatures ≥200 °C, for which the order-disorder transition occurs and the order parameter Q is close to zero [41]. However, the first changes in the Raman spectra are detectable already at 175 °C, which is lower than the soft annealing temperature used in the present study (200 ºC). Additionally, the main difference between the PDT process used for the thin film samples in the present study and the one applied in Ref. [41] on the powder samples is related to the cooling rate, which was

shown to have significant relevance to the final disorder level of the annealed samples [59]. Thus, the Q parameter of the annealed films is supposed to be higher than that of the annealed powder samples even if similar annealing temperatures were applied in both cases. Nevertheless, from the discussion presented above, and as already mentioned in the previous sub-section, the increase of the Cu/Zn disorder can safely be considered as the main effect that occurs in the CZTSe thin films under soft PDT.

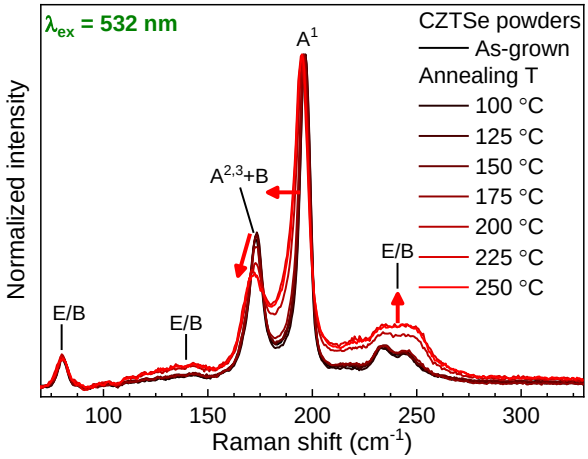

Figure 5. *Raman scattering spectra of CZTSe powder samples measured under green excitation wavelength exposed to different PDT temperatures with immediate quenching.*

A further analysis of the powder samples allows us to propose a methodology for differentiating the effect of point/cluster defects and the effect of Cu/Zn disorder using solely Raman spectra measured in backscattering configuration under 532 nm excitation wavelength (the most commonly used conditions in Raman setups). Two variables were employed for the definition of the methodology: i) the relative intensity of the Raman peaks close to 170 cm^{-1} calculated as the maximum intensity in the 165 – 180 cm^{-1} spectral range normalized to the maximum intensity in the 190 – 210 cm^{-1} spectral range that corresponds to the main kesterite peak at 195 cm^{-1}, and ii) the asymmetry of the main peak calculated as the ratio of the intensities of the fitted peaks at 192 cm^{-1} (tentatively assigned to the main peak of disordered CZTSe kesterite and responsible for the observed asymmetry) and at 195 cm^{-1} (main A symmetry peak of CZTSe kesterite). A simple fitting of the most intense band by two peaks was employed to calculate the intensity of the peaks at 192 and 195 cm^{-1}, with fixing the position of the first peak and leaving free the second one (see Figure S3 for an example of the obtained fitting). Calculating the two mentioned variables and plotting one against the other allows obtaining a discriminative graph (see Figure 6). In this graph, the powder samples show a linear-like dependence with a certain slope (see violet dots in Figure 6a). The solar cell devices of the main sample analyzed in the present study also show a similar behavior (cloud of black and red dots corresponding to the solar cells before and after first PDT, respectively). However, the points corresponding to

the non-annealed samples for the powder set and solar cells appear significantly shifted along the X-axis. This shift is due to the different composition of both sets of samples (close to stoichiometry for the powder samples [41] and Cu-poor Zn-rich for the solar cells, see *Experimental details*) leading to different densities of point/cluster defects. Taking this into account, it can be concluded that the changes in defect concentration will result in a shift only along the X-axis in the discriminative graph, while a shift along both the X and Y axes will mean mainly changes in the Cu/Zn disorder level. Additionally, a lower slope can be observed in the solar cells data compared to the powder set which may suggest a combination of Cu/Zn disorder increase (change about the X and Y axes) with additional changes in defect concentration (change about the X axis only). This, however, should be further analyzed with more details in a separate study.

In order to test the applicability of the proposed discriminative graph, previously published Raman scattering spectra of CZTSe compounds exposed to different treatments or with different chemical compositions were analysed, and the results were added in the Figure 6b:

- Ref. [47] ➔ This article reports an exhaustive Raman analysis of a compositionally-graded CZTSe sample, where the same thermal treatment was applied to the whole sample and, thus, the expected variations in the Raman spectra are related only to changes in defect concentration without significant change in Cu/Zn disorder level. The work is mainly focused on the analysis of Raman spectra measured under 325 nm excitation, but the spectra measured under 532 nm excitation are also provided in the *Supporting information* [47]. In the discriminative graph, the points associated with Ref. [47] mainly shift along the X-axis, with insignificant variation along the Y-axis, independently of the stoichiometry type (cells with composition corresponding the type A and B stoichiometric lines were selected and presented in the discriminative graph).
- Refs. [26,29,59] ➔ In these references, sets of thin films were exposed to soft PDTs. In these cases, the discriminative graph shows a clear shift along both axes, in agreement with the expected change in the Cu/Zn disorder. It is worth mentioning again that the shift along the X-axis of the non-annealed points of the different sets is mainly explained by the different concentration of defects. On the other hand, it should also be noted that the shift along the Y-axis is affected by the limitations of the Raman system which have a great influence on the width and/or asymmetry of the Raman peaks. However, this does not have a significant influence to the proposed methodology.

In this way, it can be concluded that the proposed discriminative graph allows clearly defining whether in the analysed sets of samples changes in defect concentration or changes in the Cu/Zn disorder are the dominating factor.

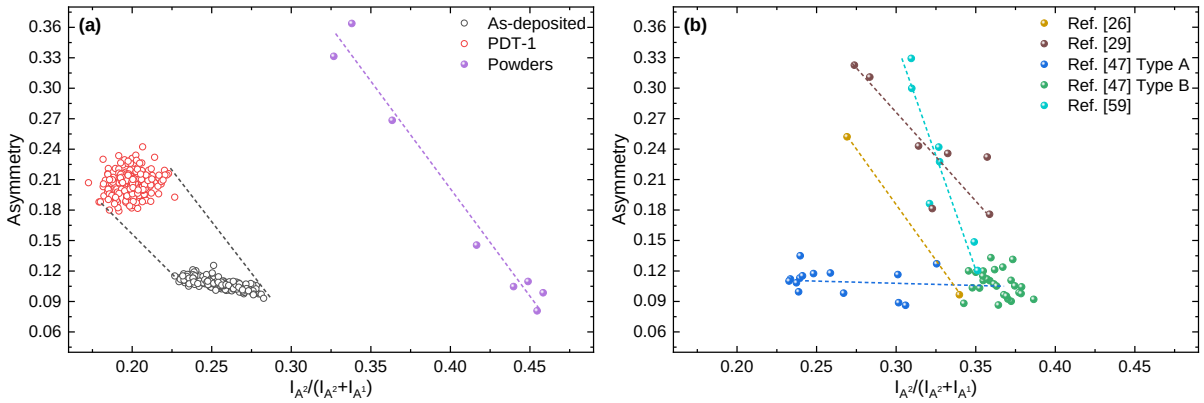

Figure 6. *Dependence of the assymetry of the A_1 symmetry peak from the relative intensity of the peaks in the range 160 – 180 cm^{-1}: (a) samples analyzed in the present work; (b) Raman spectra extracted from different references indicated in the legend. Note, that the same scale is used in both graphs for convenience.*

3.4 Thermal stability of the CdS buffer layer

As mentioned in the sub-section Evaluation of the optoelectronic properties under the soft thermal treatment, the changes in the CdS layer during the soft annealing process were the main driving force of the improved device performance, but are usually hindered by the window layer deposition conditions, especially by the relatively high temperatures employed. Moreover, the conditions of the CBD process can also significantly influence the thermal stability of the CdS layer. The specific CBD parameters used by IREC allow decreasing the CdS thickness keeping a homogeneous and compact coverage of the layer through a slow deposition rate (see *Experimental details*). As such, the observed effects in this work may be less pronounced for CdS layers deposited under different conditions. Nevertheless, in order to complete this study, an analysis of the changes that occur in this layer was also performed by means of Raman spectroscopy.

The Raman scattering measurements were performed under a 442 nm excitation wavelength which is close to resonant conditions for the CdS compound [40,67]. This allows to detect both the first and second order of the LO peak (LO components of A_1 and E_1 symmetry modes), as can be clearly observed in the results of the analysis plotted in Figure 7 (as in the previous cases, the spectra of the 56 devices are displayed as a pale diffuse spectral cloud curve and the average spectrum is shown as a legible solid line). Regarding the As-deposited devices (black line in Figure 7a), the shoulder at the low energy side of the main peak can be assigned to the TO components of the same A_1 and E_1 symmetry modes [68]. After the *PDT-1* (red line in Figure

7a) the maximum of the LO peak redshifts (see Figure S4) and there is a clear decrease of the relative intensity of the TO peaks. The red shift of the LO mode was previously observed when the grain size of the CdS increased and this was explained by a decrease of the phonon confinement effect [69]. However, this was not observed in other studies of nanostructured CdS compounds [70,71]. The presence of surface optical phonons was also mentioned as possible reason for the LO peak shift [68]. Thus a complex nature of the shift of the LO peak may also be occurring in the present case of soft PDTs. On the other hand, the observed decrease of the TO peaks was not previously reported and can be related to changes of the resonant conditions (change of the band gap due to a confinement effect). However, this should be further investigated in order to provide more insights about the nature of the observed changes in the CdS layer as a result of soft PDT. Nevertheless, both effects, together with the increased peak intensity shown in Figure 3, can be attributed to the recrystallization of the CdSwhich has a beneficial effect on the device efficiency. The improved crystalline quality of the CdS layer due to a soft PDT is also in agreement with a previously published study, where the same conclusion was made based on a PL analysis [18]. It should be noted that the most evident mark that is usually employed to detect changes of the crystalline quality from Raman spectra – change of the full width at the half maximum of the peaks (LO peak in the current case) – did not show any significant or tendency-like variation with the performed soft PDT (see Figure S4b). This should be addressed with a more detailed investigation and exceeds the goal and scope of the current study.

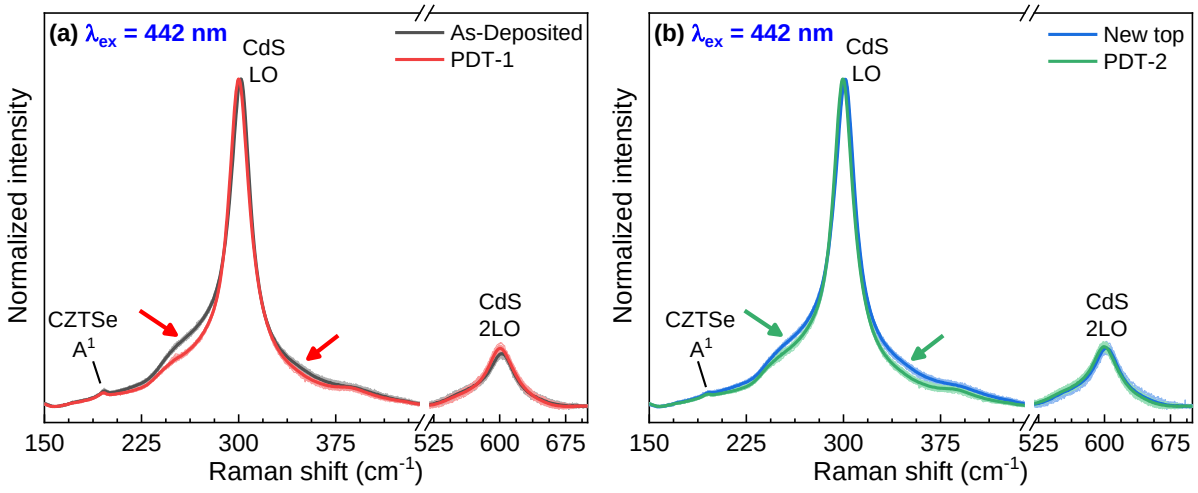

Figure 7. *Raman scattering spectra of SLG/Mo/CZTSe/CdS/i-ZnO/ITO solar cells measured under blue excitation wavelength at steps (a) As-deposited and PDT-1 and (b) New top and PDT-2 of the post deposition treatment.*

Finally, the spectra corresponding to the re-deposited CdS (*New top*) and after *PDT-2*, show completely analogous features and changes as the first ones (Figure 7b), denoting a CdS layer with similar characteristics and a similar recrystallization after PDT.

3.5 Discussion

The following main conclusions can be extracted from the overall analysis performed above:

- Soft PDTs have a critical effect on the performance of CZTSe/CdS based devices. This effect may be hindered by the final steps of device fabrication (e.g. substrate heating during front contact deposition), but still should be taken into account while producing solar cells or panels based on CZTSe/CdS heterojunctions.
- The improvement in device performance induced by the PDT in CZTSe/CdS based devices is mainly related to the improved crystalline quality of the CdS buffer layer. However, this improvement may strongly depend on the specific parameters of the CdS deposition process, which should be further investigated.
- Soft PDT processes have a strong effect on the Cu/Zn disorder in CZTSe compounds. This effect appears to have a significant impact on device performance although it was compensated by the CdS-related performance improvement. As such, this may be one of the limiting factors that prevents kesterite based PV devices to reach efficiencies higher than 13 %.

A brief literature review reveals that several groups have observed a positive effect of soft PDTs on the performance of kesterite-based thin film (in our previous works [18,29] and in Ref. [72]) and monograin [73] solar cells. However, the nature of this positive effect was ascribed to different origins. Our previous published works concluded that the main reason for the PDT-induced device efficiency improvement was related to element interdiffusion at the CZTSe/CdS interface [18,29]. Similarly, in the case of CZTS monograin solar cells, the formation of an ultrathin $Cu_2Cd_xZn_{1-x}SnS_4$ layer at the absorber/buffer interface was suggested to be the possible reason behind the beneficial effect of the PDT [73]. However, in both cases, the improved crystalline quality of the CdS buffer layer is also mentioned as a possible additional positive factor. In the present study, we directly show the high impact of the improved crystalline quality of the CdS layer. However, we cannot exclude that element interdiffusion is also playing a role in efficiency improvement, and that this can be the reason for the slightly higher defect concentration at the absorber surface after the PDT, as concluded from the discrimination graph (see Methodology for the evaluation of Cu/Zn disorder and defect evolution in CZTSe). In fact, Wang et al. observed that the annealing of CZTSe/CdS heterojunctions at temperatures ≥250°C led to an interdiffussion of elements at the heterojunction interface resulting in detrimental changes of the surface potential and an increase of the bandtailing and of Cu_{Zn}-related defects [74]. As such, similar effects but to a lesser extent

may also be occurring at the PDT temperatures employed in the present work. However, the main effects expected for elements interdiffussion (mainly Cd incorporation at the CZTSe absorber surface and Cu incorporation in the CdS layer) such as a redshift of the main CZTSe Raman mode and/or PL band as a result of the decreased bandgap [75] or a decrease of the CdS signal as a result of the increased bandgap [76] are overlapped with the effects described related to defect concentration and Cu/Zn disorder in the CZTSe and improved CdS crystallinity, respectively. In this way, more detailed and dedicated studies should be performed in order to discern the influence of elemental interdiffussion.

An interesting and open question that remains unsolved is about the Cu/Zn disorder and its effect on device performance. The possible presence of this effect was mentioned in Refs. [18] and [73] although neither of the works provided any solid proofs. In the present study, we clearly show that soft annealing in air may increase the Cu/Zn disorder in the kesterite absorbers and this has a negative effect on device efficiency. However, the crucial factor controlling the Cu/Zn disorder may not be the actual temperature of the PDT (if it is around the critical temperature of order-disorder transition), but rather the cooling rate. The fast quenching performed in powder samples allowed to "freeze" the increased disorder in kesterites [41], while slow cooling (with cooling rate <1 °C/min) resulted in almost ordered CZTSe [59]. A similar disorder decrease effect was shown also to happen as a result of long time PDTs at temperatures significantly lower than the critical transition temperature (>10 h at <140 °C) [59,72]. The latest work based on first-principle calculations shows that disorder by itself has low influence on device performance, but it reduces the formation energy of detrimental deep Sn_{Zn} and Sn_{Cu} defects [77], thus having an important role during the synthesis of kesterite absorbers. Nevertheless, all the latest studies on soft PDTs in CdS/kesterite based devices (in the temperature limits 100 – 200 °C), including the present investigation, show a quite low thermal stability of this absorber and of the absorber/buffer interface (with several positive and/or negative effects taking place), and this should be taken into account not only at the final stages of the device preparation (deposition of window layer or device encapsulation), but even during the device operation (the working temperature of solar modules can exceed 100 °C during operation) [78,79].

4. Conclusions

The present study has assessed the thermal stability of the CZTSe/CdS heterojunction in SLG/Mo/CZTSe/CdS/i-ZnO/ITO devices under soft PDTs. For this purpose, a series of PDT

steps and a comprehensive characterization performed at each of them by means of Raman and PL spectroscopies coupled with optoelectronic analysis allowed to clearly differentiate the effect of soft PDT on the buffer and absorber layers of full CZTSe-based devices. The high statistical analysis of the optoelectronic properties of the solar cells (>50 cells were analyzed at each step) allows concluding that the main driving force leading to the enhancement of the device efficiency after PDT is the improvement of the CdS buffer layer, while the CZTSe absorber shows a rather negative impact on device efficiency. On the one hand, the analysis of the Raman scattering spectra of the CdS buffer layer measured in resonant conditions reveals the recrystallization of this nanometric layer as the possible main actor playing a positive role in the observed increase of solar cell efficiency after PDT. On the other hand, the analysis of both Raman and PL spectra of the absorber layer shows an increase of the Cu/Zn disordering after the soft PDT, which plays rather negative role on device performance. The thermal instability at low temperatures presented in this work represents a limiting factor that needs to be taken into consideration for the further development of the kesterite-based PV technology. These conclusions are supported by the analysis of an additional set of highly homogeneous powder samples with different Cu/Zn disorder level that has allowed to propose a fast methodology based solely on Raman scattering spectroscopy for easily discerning between changes in the disorder level and in the concentration of point defects in kesterite samples.

Acknowledgements

The project on which these results are based has received funding from the European Union's Horizon 2020 research and innovation programme under grant agreements no 777968 (INFINITE-CELL project) and 952982 (Custom-Art project). This project has received funding from the European Union’s Horizon 2020 research and innovation programme under Marie Skłodowska-Curie grant agreement No. 801342 (Tecniospring INDUSTRY) and the Government of Catalonia’s Agency for Business Competitiveness (ACCIÓ). Authors from IREC belong to the SEMS (Solar Energy Materials and Systems) Consolidated Research Group of the “Generalitat de Catalunya” (ref. 2017 SGR 862) and are grateful to European Regional Development Funds (ERDF, FEDER Programa Competitivitat de Catalunya 2007–2013). M.G. acknowledges the financial support from Spanish Ministry of Science, Innovation and Universities within the Juan de la Cierva fellowship (IJC2018-038199-I). S.G thanks the grant IJC2020-044716-I funded by MCIN/AEI/ 10.13039/501100011033 and by the European Union NextGenerationEU/PRTR.

References

[1] Solar Frontier Achieves World Record Thin-Film Solar Cell Efficiency: 22.3%, https://www.solar-frontier.eu/uploads/media/SFE-Thin-Film-Solar-Cell-Efficiency-EN.pdf, 2015 (accessed 19 July 2022).

[2] First Solar achieves yet another cell conversion efficiency world record, https://investor.firstsolar.com/news/press-release-details/2016/First-Solar-Achieves-Yet-Another-Cell-Conversion-Efficiency-World-Record/default.aspx, 2016 (accessed 19 July 2022).

[3] C. Candelise, M. Winskel, R. Gross, Implications for CdTe and CIGS technologies production costs of indium and tellurium scarcity: Effects of indium and tellurium scarcity, Prog. Photovolt. Res. Appl. 20 (2012) 816–831. https://doi.org/10.1002/pip.2216.

[4] A. Feltrin, A. Freundlich, Material considerations for terawatt level deployment of photovoltaics, Renew. Energy 33 (2008) 180–185. https://doi.org/10.1016/j.renene.2007.05.024.

[5] G. Phipps, C. Mikolajczak, T. Guckes, Indium and gallium: long-term supply, Renew. Energy Focus. 9 (2008) 56–59. https://doi.org/10.1016/S1471-0846(08)70140-9.

[6] I. Becerril-Romero, Alternative substrates for sustainable and Earth-abundant thin film photovoltaics, Universitat de Barcelona, 2019. http://diposit.ub.edu/dspace/bitstream/2445/147001/1/IBR_PhD_THESIS.pdf.

[7] W. Wang, M.T. Winkler, O. Gunawan, T. Gokmen, T.K. Todorov, Y. Zhu, D.B. Mitzi, Device Characteristics of CZTSSe Thin-Film Solar Cells with 12.6% Efficiency, Adv. Energy Mater. 4 (2014)1301465. https://doi.org/10.1002/aenm.201301465.

[8] Jiazheng Zhou, Xiao Xu, Biwen Duan, Huijue Wu, Jiangjian Shi, Yanhong Luo, Dongmei Li, Qingbo Meng, Regulating crystal growth via organic lithium salt additive for efficient Kesterite solar cells, Nano Energy 89 (2021) 106405. https://doi.org/10.1016/j.nanoen.2021.106405.

[9] U. Rau, D. Braunger, R. Herberholz, H.W. Schock, J.-F. Guillemoles, L. Kronik, D. Cahen, Oxygenation and air-annealing effects on the electronic properties of Cu(In,Ga)Se_2 films and devices, J. Appl. Phys. 86 (1999) 497–505. https://doi.org/10.1063/1.370758.

[10] I. Khatri, K. Shudo, J. Matsuura, M. Sugiyama, T. Nakada, Impact of heat-light soaking on potassium fluoride treated CIGS solar cells with CdS buffer layer, Prog. Photovoltaics Res. Appl. 26 (2018) 171–178. https://doi.org/10.1002/pip.2962.

[11] I. Khatri, J. Matsuura, M. Sugiyama, T. Nakada, Effect of heat-bias soaking on cesium fluoride-treated CIGS thin film solar cells, Prog. Photovoltaics Res. Appl. 27 (2019) 22–29. https://doi.org/10.1002/pip.3067.

[12] J. Matsuura, I. Khatri, T. Lin, M. Sugiyama and T. Nakada, Impact of heat-light soaking and heat-bias soaking on NaF-treated CIGS thin film solar cells, Prog. Photovoltaics Res. Appl. 27 (2019) 623–629. https://doi.org/10.1002/pip.3135.

[13] I. Repins, M.A. Contreras, B. Egaas, C. DeHart, J. Scharf, C.L. Perkins, B. To, R. Noufi, 19.9%-efficient ZnO/CdS/CuInGaSe_2 solar cell with 81.2% fill factor, Prog. Photovolt. Res. Appl 16 (2008) 235–239. https://doi.org/10.1002/pip.822.

[14] D. Hauschild, F. Meyer, A. Benkert, D. Kreikemeyer-Lorenzo, S. Pohlner, J. Palm, M. Blum, W. Yang, R.G. Wilks, M. Bär, C. Heske, L. Weinhardt, F. Reinert, Annealing-

induced effects on the chemical structure of the In_2S_3/CuIn(S,Se)$_2$ thin-film solar cell interface, J. Phys. Chem. C 119 (2015) 10412–10416. https://doi.org/10.1021/acs.jpcc.5b01622.

[15] J.H. Kim, S. Choi, M. Choi, T. Gershon, Y.S. Lee, W. Wang, B. Shin, S. Chung, Atomic-Scale Observation of Oxygen Substitution and Its Correlation with Hole-Transport Barriers in $Cu_2ZnSnSe_4$ Thin-Film Solar Cells, Adv. Energy Mater. 6 (2016) 1501902. https://doi.org/10.1002/aenm.201501902.

[16] K. Sardashti, R. Haight, T. Gokmen, W. Wang, L. Chang, D.B. Mitzi, A.C. Kummel, Impact of Nanoscale Elemental Distribution in High-Performance Kesterite Solar Cells, Adv. Energy Mater. 5 (2015) 1402180. https://doi.org/10.1002/aenm.201402180.

[17] M.G. Sousa, A.F. Da Cunha, J.P. Teixeira, J.P. Leitão, G. OteroIrurueta and M.K. Singh, Optimization of post-deposition annealing in Cu_2ZnSnS_4 thin film solar cells and its impact on device performance, Sol. Energy Mater. Sol. Cells 170 (2017) 287–294. https://doi.org/10.1016/j.solmat.2017.05.065.

[18] M. Neuschitzer, Y. Sanchez, T. Olar, T. Thersleff, S. Lopez-Marino, F. Oliva, M. Espindola-Rodriguez, H. Xie, M. Placidi, V. Izquierdo-Roca, Complex Surface Chemistry of Kesterites: Cu/Zn Reordering after Low Temperature Postdeposition Annealing and Its Role in High Performance Devices, Chem. Mater. 27 (2015) 5279–5287. https://doi.org/10.1021/acs.chemmater.5b01473.

[19] R. Haight, X. Shao, W. Wang, D.B. Mitzi, Electronic and elemental properties of the $Cu_2ZnSn(S,Se)_4$ surface and grain boundaries, Appl. Phys. Lett., 2014, 104, 033902. https://doi.org/10.1063/1.4862791.

[20] G. Rey, T.P. Weiss, J. Sendler, A. Finger, C. Spindler, F. Werner, M. Melchiorre, M. Hala, M. Guennou and S. Siebentritt, Ordering kesterite improves solar cells: A low temperature post-deposition annealing study, Sol. Energy Mater. Sol. Cells 151 (2016) 131–138. https://doi.org/10.1016/j.solmat.2016.02.014.

[21] C. Krämmer, C. Huber, C. Zimmermann, M. Lang, T. Schnabel, T. Abzieher, E. Ahlswede, H. Kalt, M. Hetterich, Reversible order-disorder related band gap changes in $Cu_2ZnSn(S,Se)_4$ via post-annealing of solar cells measured by electroreflectance, Appl. Phys. Lett. 105 (2014) 262104. https://doi.org/10.1063/1.4905351.

[22] J.K. Larsen, F. Larsson, T. Törndahl, N. Saini, L. Riekehr, Y. Ren, A. Biswal, D. Hauschild, L. Weinhardt, C. Heske, C. Platzer Björkman, Cadmium Free Cu_2ZnSnS_4 Solar Cells with 9.7% Efficiency, Adv. Energy Mater. 9 (2019) 1900439. https://doi.org/10.1002/aenm.201900439.

[23] H. Xie, S. López-Marino, T. Olar, Y. Sánchez, M. Neuschitzer, F. Oliva, S. Giraldo, V. Izquierdo-Roca, I. Lauermann, A. Perez-Rodriguez, Impact of Na Dynamics at the $Cu_2ZnSn(S,Se)_4$/CdS Interface During Post Low Temperature Treatment of Absorbers, ACS Appl. Mater. Interfaces 8 (2016) 5017–5024. https://doi.org/10.1021/acsami.5b12243.

[24] J.J.S. Scragg, J.K. Larsen, M. Kumar, C. Persson, J. Sendler, S. Siebentritt, C. Platzer Björkman, Cu–Zn disorder and band gap fluctuations in $Cu_2ZnSn(S,Se)_4$: Theoretical and experimental investigations, Phys. Status Solidi B 253 (2016) 247–254. https://doi.org/10.1002/pssb.201552530.

[25] J.J.S. Scragg, L. Choubrac, A. Lafond, T. Ericson, C. Platzer Björkman, A low-temperature order-disorder transition in Cu_2ZnSnS_4 thin films, Appl. Phys. Lett. 104 (2014) 041911. https://doi.org/10.1063/1.4863685.
[26] G. Rey, A. Redinger, J. Sendler, T.P. Weiss, M. Thevenin, M. Guennou, B.E.l. Adib, S. Siebentritt, The band gap of $Cu_2ZnSnSe_4$: Effect of order-disorder, Appl. Phys. Lett. 105 (2014) 112106. https://doi.org/10.1063/1.4896315.
[27] A. Crovetto, O. Hansen, What is the band alignment of $Cu_2ZnSn(S,Se)_4$ solar cells?, Sol. Energy Mater. Sol. Cells 169 (2017) 177–194. https://doi.org/10.1016/j.solmat.2017.05.008
[28] S. Giraldo, E. Saucedo, M. Neuschitzer, F. Oliva, M. Placidi, X. Alcobé, V. Izquierdo-Roca, S. Kim, H. Tampo, H. Shibata, How small amounts of Ge modify the formation pathways and crystallization of kesterites, Energy Environ. Sci. 11 (2018) 582–593. https://doi.org/10.1039/C7EE02318A.
[29] Mirjana Dimitrievska, Sergio Giraldo, Paul Pistor, Edgardo Saucedo, Alejandro Pérez-Rodríguez, Victor Izquierdo-Roca, Raman scattering analysis of the surface chemistry of kesterites: Impact of post-deposition annealing and Cu/Zn reordering on solar cell performance, Sol. Energy Mater. Sol. Cells 157 (2016) 462–467. https://doi.org/10.1016/j.solmat.2016.07.009.
[30] Marit Kauk-Kuusik, Kristi Timmo, Katri Muska, Maris Pilvet, Jüri Krustok, Raavo Josepson, Guy Brammertz, Bart Vermang, Mati Danilson, Maarja Grossberg, Detailed Insight into the CZTS/CdS Interface Modification by Air Annealing in Monograin Layer Solar Cells, ACS Appl. Energy Mater. 4 (2021) 12374–12382. https://doi.org/10.1021/acsaem.1c02186.
[31] C. Yan, J. Huang, K. Sun, S. Johnston, Y. Zhang, H. Sun, A. Pu, M. He, F. Liu, K. Eder, L. Yang, J.M. Cairney, N.J. Ekins-Daukes, Z. Hameiri, J.A. Stride, S. Chen, M.A. Green, X. Hao, Cu_2ZnSnS_4 solar cells with over 10% power conversion efficiency enabled by heterojunction heat treatment, Nat. Energy 3 (2018) 764–772. https://doi.org/10.1038/s41560-018-0206-0.
[32] C. Malerba, M. Valentini, A. Mittiga, Cation Disorder In Cu_2ZnSnS_4 Thin Films: Effect On Solar Cell Performances, Sol. RRL 1 (2017) 1700101. https://doi.org/10.1002/solr.201700101
[33] Z. Su, G. Liang, P. Fan, J. Luo, Z. Zheng, Z. Xie, W. Wang, S. Chen, J. Hu, Y. Wei, Device Postannealing Enabling over 12% Efficient Solution-Processed Cu_2ZnSnS_4 Solar Cells with Cd^{2+} Substitution, Adv. Mater. 32 (2020) 2000121. https://doi.org/10.1002/adma.202000121.
[34] S. Gao, Y. Zhang, J. Ao, X. Li, S. Qiao, Y. Wang, S. Lin, Z. Zhang, D. Wang, Z. Zhou, Insight into the role of post-annealing in air for high efficient $Cu_2ZnSn(S,Se)_4$ solar cells, Sol. Energy Mater. Sol. Cells 182 (2018) 228–236. https://doi.org/10.1016/j.solmat.2018.03.029
[35] M.G. Gang, S.W. Shin, M.P. Suryawanshi, U.V. Ghorpade, Z. Song, J.S. Jang, J.H. Yun, H. Cheong, Y. Yan, J.H. Kim, Band Tail Engineering in Kesterite $Cu_2ZnSn(S,Se)_4$ Thin-Film Solar Cells with 11.8% Efficiency, J. Phys. Chem. Lett. 9 (2018) 4555–4561. https://doi.org/10.1021/acs.jpclett.8b01433.
[36] K. Sugimoto, T. Ebi, N. Suyama, K. Nakada, A. Yamada, Separation of effects of InGaN/GaN superlattice on performance of light-emitting diodes using mid-

temperature-grown GaN layer, Jpn. J. Appl. Phys. 57 (2018) 062101. https://doi.org/10.7567/JJAP.57.062101.

[37] S. Tajima, M. Umehara, M. Hasegawa, T. Mise, T. Itoh, Cu_2ZnSnS_4 photovoltaic cell with improved efficiency fabricated by high-temperature annealing after CdS buffer-layer deposition, Prog. Photovoltaics Res. Appl. 25 (2017) 14–22. https://doi.org/10.1002/pip.2837.

[38] S. López-Marino, M. Placidi, A. Pérez-Tomás, J. Llobet, V. Izquierdo-Roca, X. Fontané, A. Fairbrother, M. Espíndola-Rodríguez, D. Sylla, A. Pérez-Rodríguez, E. Saucedo, Inhibiting the absorber/Mo-Back Contact Decomposition Reaction in $Cu_2ZnSnSe_4$ Solar Cells: The Role of a ZnO Intermediate Nanolayer, J. Mater. Chem. A 1 (2013) 8338−8343. https://doi.org/10.1039/C3TA11419H.

[39] Sergio Giraldo, Zacharie Jehl, Marcel Placidi, Victor Izquierdo-Roca, Alejandro Pérez-Rodríguez, Edgardo Saucedo, Progress and Perspectives of Thin Film Kesterite Photovoltaic Technology: A Critical Review, Advanced Materials 31 (2019) 1806692. https://doi.org/10.1002/adma.201806692.

[40] V. Hernández-Calderón, O. Vigil-Galán, M. Guc, A. Carrillo-Osuna, S. Ramírez-Velasco, F.J. Sánchez-Rodríguez, P. Vidal-Fuentes, S. Giraldo, E. Saucedo, Y. Sánchez, CdS/ZnS Bilayer Thin Films Used As Buffer Layer in 10%-Efficient $Cu_2ZnSnSe_4$ Solar Cells, ACS Appl. Energy Mater. 3 (2020) 6815−6823. https://doi.org/10.1021/acsaem.0c00937.

[41] Daniel M. Többens, Galina Gurieva, Sergiu Levcenko, Thomas Unold, Susan Schorr, Temperature dependency of Cu/Zn ordering in CZTSe kesterites determined by anomalous diffraction, Phys. Status Solidi B 253 (2016) 1890–1897. https://doi.org/10.1002/pssb.201600372.

[42] Florian Oliva, Steffen Kretzschmar, Diego Colombara, Sara Tombolato, Carmen Maria Ruiz, Alex Redinger, Edgardo Saucedo, Cédric Broussilloue, Thomas Goislard de Monsabert, Thomas Unold, Philip J. Dale, Victor Izquierdo-Roca, Alejandro Pérez-Rodríguez, Optical methodology for process monitoring of chalcopyrite photovoltaic technologies: Application to low cost $Cu(In,Ga)(S,Se)_2$ electrodeposition based processes, Sol. Energy Mater. Sol. Cells 158 (2016) 168–183. https://doi.org/10.1016/j.solmat.2015.12.036.

[43] Florian Oliva, Laia Arqués, Laura Acebo, Maxim Guc, Yudania Sánchez, Xavier Alcobé, Alejandro Perez-Rodriguez, Edgardo Sauce, Victor Izquierdo-Roca, Characterization of Cu_2SnS_3 polymorphism and its impact on optoelectronic properties, J. Mater. Chem. A 5 (2017) 23863–23871. https://doi.org/10.1039/C7TA08705E.

[44] Maxim Guc, Florian Oliva, Rokas Kondrotas, Xavier Alcobe, Marcel Placidi, Paul Pistor, Edgardo Saucedo, Alejandro Perez-Rodriguez, Victor Izquierdo-Roca, $CuZnInSe_3$-based solar cells: Impact of copper concentration on vibrational and structural properties and device performance, Prog. Photovoltaics Res. Appl. 27 (2019) 716–723. https://doi.org/10.1002/pip.3150.

[45] Maxim Guc, Jacob Andrade-Arvizu, Ibbi Y. Ahmet, Florian Oliva, Marcel Placidi, Xavier Alcobé, Edgardo Saucedo, Alejandro Pérez-Rodríguez, Andrew L. Johnson, Victor Izquierdo-Roca, Structural and vibrational properties of α- and π-SnS polymorphs for photovoltaic applications, Acta Materialia 183 (2020) 1–10. https://doi.org/10.1016/j.actamat.2019.11.016.

[46] Susan Schorr, Galina Gurieva, Maxim Guc, Mirjana Dimitrievska, Alejandro Pérez-Rodríguez, Victor Izquierdo-Roca, Claudia S Schnohr, Juran Kim, William Jo, Jose Manuel Merino, Point defects, compositional fluctuations and secondary phases in non-stoichiometric kesterites, J. Phys. Energy 2 (2020) 012002. https://doi.org/10.1088/2515-7655/ab4a25.

[47] Mirjana Dimitrievska, Florian Oliva, Maxim Guc, Sergio Giraldo, Edgardo Saucedo, Alejandro Pérez-Rodríguez, Victor Izquierdo-Roca, Defect characterisation in $Cu_2ZnSnSe_4$ kesterites via resonance Raman spectroscopy and the impact on optoelectronic solar cell properties, J. Mater. Chem. A 7 (2019) 13293–13304. https://doi.org/10.1039/C9TA03625C.

[48] Enric Grau-Luque, Ikram Anefnaf, Nada Benhaddou, Robert Fonoll-Rubio, Ignacio Becerril-Romero, Safae Aazou, Edgardo Saucedo, Zouheir Sekkat, Alejandro Perez-Rodriguez, Victor Izquierdo-Roca, Maxim Guc, Combinatorial and machine learning approaches for the analysis of $Cu_2ZnGeSe_4$: influence of the off-stoichiometry on defect formation and solar cell performance, J. Mater. Chem. A 9 (2021) 10466–10476. https://doi.org/10.1039/D1TA01299A

[49] K. Wang, O. Gunawan, T. Todorov, B. Shin, S.J. Chey, N.A. Bojarczuk, D. Mitzi, S. Guha, Thermally evaporated Cu_2ZnSnS_4 solar cells, Appl. Phys. Lett. 97 (2010) 143508. http://dx.doi.org/10.1063/1.3499284.

[50] G. Brammertz, M. Buffière, S. Oueslati, H. ElAnzeery, K. Ben Messaoud, S. Sahayaraj, C. Köble, M. Meuris, J. Poortmans, Characterization of defects in 9.7% efficient $Cu_2ZnSnSe_4$-CdS-ZnO solar cells, Appl. Phys. Lett. 103 (2013) 163904. https://doi.org/10.1063/1.4826448.

[51] Jie Zhong, Zhe Xia, Miao Luo, Juan Zhao, Jie Chen, Liang Wang, Xinsheng Liu, Ding-Jiang Xue, Yi-Bing Cheng, Haisheng Song, Jiang Tang, Sulfurization induced surface constitution and its correlation to the performance of solution-processed $Cu_2ZnSn(S,Se)_4$ solar cells, Sci. Rep. 4 (2014) 6288. https://doi.org/10.1038/srep06288.

[52] M. Buffière, G. Brammertz, M. Batuk, C. Verbist, D. Mangin, C. Koble, J. Hadermann, M. Meuris, J. Poortmans, Microstructural analysis of 9.7% efficient $Cu_2ZnSnSe_4$ thin film solar cells, Appl. Phys. Lett. 105 (2014) 183903. http://dx.doi.org/10.1063/1.4901401.

[53] Xinchen Li, Daming Zhuang, Ning Zhang, Ming Zhao, Xinping Yu, Peng Liu, Yaowei Wei, Guoan Rena, Achieving 11.95% efficient $Cu_2ZnSnSe_4$ solar cells fabricated by sputtering a Cu–Zn–Sn–Se quaternary compound target with a selenization process, J. Mater. Chem. A 7 (2019) 9948–9957. https://doi.org/10.1039/C9TA00385A.

[54] Chuanhe Ma, Xiaoshuang Lu, Bin Xu, Fei Zhao, Xueer An, Bo Li, Fangyu Yue, Jinchun Jiang, Ye Chen, Lin Sun, Junhao Chu, Effect of CZTS/CdS interfaces deposited with sputtering and CBD methods on V_{oc} deficit and efficiency of CZTS solar cells, J. Alloy Compd. 817 (2020) 153329. https://doi.org/10.1016/j.jallcom.2019.153329.

[55] M. Guc, S. Levcenko, V. Izquierdo-Roca, X. Fontane, E. Arushanov, A. Pérez-Rodríguez, Polarized Raman scattering analysis of $Cu_2ZnSnSe_4$ and $Cu_2ZnGeSe_4$ single crystals, J. Appl. Phys. 114 (2013) 193514. https://doi.org/10.1063/1.4830028.

[56] Mirjana Dimitrievska, Andrew Fairbrother, Edgardo Saucedo, Alejandro Pérez-Rodríguez, Victor Izquierdo-Roca, Influence of compositionally induced defects on the vibrational properties of device grade $Cu_2ZnSnSe_4$ absorbers for kesterite based solar cells, Appl. Phys. Lett. 106 (2015) 073903. https://doi.org/10.1063/1.4913262.

[57] M. Valentini, C. Malerba, F. Menchini, D. Tedeschi, A. Polimeni, M. Capizzi, A. Mittiga, Effect of the order-disorder transition on the optical properties of Cu_2ZnSnS_4, Appl. Phys. Lett. 108 (2016) 211909. https://doi.org/10.1063/1.4952973.

[58] Taavi Raadik, Jüri Krustok, M. Kauk-Kuusik, K. Timmo, M. Grossberg, K. Ernits, J. Bleuse, Low temperature time resolved photoluminescence in ordered and disordered Cu_2ZnSnS_4 single crystals, Physica B 508 (2017) 47–50. https://doi.org/10.1016/j.physb.2016.12.011.

[59] Christiane Stroth, Mohamed H. Sayed, Janet Neerken, Ulf Mikolajczak, Germain Rey, Jürgen Parisi, Levent Gütay, In-situ investigation of the order-disorder transition in $Cu_2ZnSnSe_4$ by optical transmission spectroscopy, AIP Adv. 7 (2017) 025303. https://doi.org/10.1063/1.4976619.

[60] S. Levcenko, V.E. Tezlevan, E. Arushanov, S. Schorr, T. Unold, Free-to-bound recombination in near stoichiometric Cu_2ZnSnS_4 single crystals, Phys. Rev. B 86 (2012) 045206. https://doi.org/10.1103/PhysRevB.86.045206.

[61] M. Guc, R. Caballero, K.G. Lisunov, N. López, E. Arushanov, J.M. Merino, M. León, Disorder and variable-range hopping conductivity in Cu_2ZnSnS_4 thin films prepared by flash evaporation and post-thermal treatment, J. Alloy Compd. 596 (2014) 140–144. https://doi.org/10.1016/j.jallcom.2014.01.177.

[62] Shiyou Chen, Aron Walsh, Xin-Gao Gong, Su-Huai Wei, Classification of Lattice Defects in the Kesterite Cu_2ZnSnS_4 and $Cu_2ZnSnSe_4$ Earth-Abundant Solar Cell Absorbers, Adv. Mater. 25 (2013) 1522–1539. https://doi.org/10.1002/adma.201203146.

[63] Laura Elisa Valle Rios, Kai Neldner, Galina Gurieva, Susan Schorr, Existence of off-stoichiometric single phase kesterite, J. Alloy Compd. 657 (2016) 408–413. https://doi.org/10.1016/j.jallcom.2015.09.198.

[64] M.Y. Valakh, O.F. Kolomys, S.S. Ponomaryov, V.O. Yukhymchuk, I.S. Babichuk, V. Izquierdo-Roca, E. Saucedo, A. Perez-Rodriguez, J.R. Morante, S. Schorr, I.V. Bodnar, Raman scattering and disorder effect in Cu_2ZnSnS_4, Phys. Status Solidi RRL 7 (2013) 258–261. https://doi.org/10.1002/pssr.201307073.

[65] R. Caballero, E. Garcia-Llamas, J.M. Merino, M. León, I. Babichuk, V. Dzhagan, V. Strelchuk and M. Valakh, Non-stoichiometry effect and disorder in Cu_2ZnSnS_4 thin films obtained by flash evaporation: Raman scattering investigation, Acta Materialia 65 (2014) 412–417. https://doi.org/10.1016/j.actamat.2013.11.010.

[66] Maxim Guc, Eduard Bailo, Robert Fonoll-Rubio, Fabien Atlan, Marcel Placidi, Philip Jackson, Dimitrios Hariskos, Xavier Alcobe, Paul Pistore, Ignacio Becerril-Romero, Alejandro Perez-Rodriguez, Francisco Ramos, Victor Izquierdo-Rocaa, Evaluation of defect formation in chalcopyrite compounds under Cu-poor conditions by advanced structural and vibrational analyses, Acta Materialia 223 (2022) 117507. https://doi.org/10.1016/j.actamat.2021.117507.

[67] R.C.C. Leite, J.F. Scott, T.C. Damen, Multiple-Phonon Resonant Raman Scattering in CdS, Phys. Rev. Lett. 22 (1969) 780–782. https://doi.org/10.1103/PhysRevLett.22.780.

[68] J. Trajić, M. Gilić, N. Romčević, M. Romčević, G. Stanišić, B. Hadžić, M. Petrović, Y.S. Yahia, Raman spectroscopy of optical properties in CdS thin films, Sci. Sintering 47 (2015) 145–152. https://doi.org/10.2298/SOS1502145T.

[69] D. Routkevitch, T.L. Haslett, L. Ryan, T. Bigioni, C. Douketis, M. Moskovits, Synthesis and resonance Raman spectroscopy of CdS nano-wire arrays, Chem. Phys. 210 (1996) 343–352. https://doi.org/10.1016/0301-0104(96)00171-1.

[70] J.J. Shiang, S.H. Risbud, A.P. Alivisatos, Resonance Raman studies of the ground and lowest electronic excited state in CdS nanocrystals, J. Chem. Phys. 98 (1993) 8432. https://doi.org/10.1063/1.464501.

[71] L. Zeiri, I. Patla, S. Acharya, Y. Golan, S. Efrima, Raman Spectroscopy of Ultranarrow CdS Nanostructures, J. Phys. Chem. C 111 (2007) 11843–11848. https://doi.org/10.1021/jp072015q.

[72] Michael A. Lloyd, Xiangyu Ma, Austin G. Kuba, Brian E. McCandless, Matthew F. Doty, Robert Birkmire, Effects of composition and thermal treatment on V_{OC}-limiting defects in single-crystalline $Cu_2ZnSnSe_4$ solar cells, Prog. Photovoltaics Res. Appl. 30 (2022) 503–517. https://doi.org/10.1002/pip.3516.

[73] Marit Kauk-Kuusik, Kristi Timmo, Katri Muska, Maris Pilvet, Jüri Krustok, Raavo Josepson, Guy Brammertz, Bart Vermang, Mati Danilson, Maarja Grossberg, Detailed Insight into the CZTS/CdS Interface Modification by Air Annealing in Monograin Layer Solar Cells, ACS Appl. Energy Mater. 4 (2021) 12374–12382. https://doi.org/10.1021/acsaem.1c02186.

[74] S. Wang, Z. Shen, Y. Sun, H. Li, K. Zhang, L. Wu, J. Ao, Y. Zhang, Defects and Surface Electrical Property Transformation Induced by Elemental Interdiffusion at the p−n Heterojunction via HighTemperature Annealing, ACS Appl. Mater. Interfaces 13 (2021) 12211−12220. https://doi.org/10.1021/acsami.1c00096

[75] Shreyash Hadke, Wei Chen, Joel Ming Rui Tan, Maxim Guc, Victor Izquierdo-Roca, Gian-Marco Rignanese, Geoffroy Hautier, Lydia Helena Wong, Effect of Cd on cation redistribution and order-disorder transition in $Cu_2(Zn,Cd)SnS_4$, J. Mater. Chem. A 7 (2019) 26927–26933. https://doi.org/10.1039/C9TA09572A.

[76] Y. Sánchez, M. Neuschitzer, M. Dimitrievska, M. Espíndola-Rodríguez, J. López-García, V. Izquierdo-Roca, O. Vigil-Galán, E. Saucedo, High V_{OC} $Cu_2ZnSnSe_4$/CdS:Cu based solar cell: Evidences of a metal-insulator-semiconductor (MIS) type hetero-junction, 2014 IEEE 40th Photovoltaic Specialist Conference (PVSC) 2014, pp. 0417-0420. https://doi.org/10.1109/PVSC.2014.6924948.

[77] Wei Chen, Diana Dahliah, Gian-Marco Rignanese and Geoffroy Hautier, Origin of the low conversion efficiency in Cu_2ZnSnS_4 kesterite solar cells: the actual role of cation disorder, Energy Environ. Sci. 14 (2021) 3567–3578. https://doi.org/10.1039/D1EE00260K.

[78] D. Faiman, Assessing the outdoor operating temperature of photovoltaic modules, Prog. Photovoltaics Res. Appl. 16 (2008) 307–315. https://doi.org/10.1002/pip.813.

[79] W. Yuan, J. Ji, Z. Li, F. Zhou, X. Ren, X. Zhao, S. Liu, Comparison study of the performance of two kinds of photovoltaic/thermal(PV/T) systems and a PV module at high ambient temperature, Energy 148 (2018) 1153–1161. https://doi.org/10.1016/j.energy.2018.01.121.